RSC Advances

PAPER

View Article Online
View Journal | View Issue

Cite this: *RSC Adv.*, 2025, **15**, 41959

Plasmonic effect-driven strategy for boosting photoelectrocatalytic degradation of rhodamine B using a SnS_2/Au self-supported photoelectrode

Yuanyuan Tian, * Qianqian Zhang, Jianjun Zhang, Chao Ren and Xixin Liu

Photoelectrocatalytic degradation of pollutants is regarded as one of the green disposal schemes for water pollutants under the "dual carbon" strategy. In this paper, a gold-based tin disulfide self-supporting photoelectrode (SnS_2–Au/Ti foil) was successfully prepared by a two-step method and applied to the photoelectrocatalytic degradation of rhodamine B (RhB) pollutants. The phase structure of the self-supported photoelectrode was characterized by scanning electron microscopy, X-ray diffraction, ultraviolet-visible spectrophotometry, and fluorescence spectrophotometry. The test results for photoelectrocatalytic degradation performance demonstrated that the degradation performance of the pollutant RhB was significantly enhanced *via* the plasmonic effect of gold in synergy with the intrinsic photocatalytic characteristics of the tin sulfide semiconductor. The photoelectrocatalytic degradation efficiency of the self-supported photoelectrode reached 81.25% within 120 minutes. The composite electrode SnS_2–Au/Ti foil demonstrated an 38.18% and 8.45% increase in photoelectrocatalytic degradation of RhB efficiency over the single Au and SnS_2 electrodes, respectively. The plasmonic effect-driven strategy for boosting photoelectrocatalytic efficiency opens new perspectives for RhB degradation.

Received 13th June 2025
Accepted 15th October 2025

DOI: 10.1039/d5ra04205d

rsc.li/rsc-advances

1 Introduction

Driven by rapid industrialization and urbanization, the surging global energy demand has exacerbated environmental degradation, particularly through escalating pollutant emissions. Among these pollutants, Rhodamine B (RhB), a synthetic cationic dye widely used in the textile, paper, and leather industries, has garnered significant attention owing to its resistance to natural degradation and its potent biotoxicity.[1,2] It is classified by the World Health Organization as a Group 3 carcinogen.[3] Currently, the degradation treatment of RhB primarily relies on four main methodologies: photocatalytic oxidation, Fenton and Fenton-like methods,[4,5] combined degradation agents, and biological synergy techniques.[6] However, the presence of secondary pollution, high costs, and low degradation efficiency, among other issues, presents substantial challenges in establishing a green and efficient pathway for rhodamine B degradation. Photoelectrocatalytic degradation technology represents a green and highly efficient degradation approach that leverages the synergistic effects of solar energy and electrical energy. This technology has been extensively applied to degrade methylene blue[7–9] and various other toxic and hazardous substances. The design and fabrication of photoelectrodes are critical factors in determining the efficiency and effectiveness of photoelectrocatalytic degradation processes.

Tin disulfide (SnS_2) semiconductor material ($E_g \approx 2.2$ eV) exhibits effective visible-light absorption and is widely utilized for photocatalysts.[10] Shuai *et al.* successfully synthesized Mn-doped SnS_2 photocatalysts, which significantly enhanced the performance of photocatalytic degradation of RhB.[11] Chen *et al.* prepared SnS_2/CPAN nanocomposites by compounding cyclized polyacrylonitrile (CPAN), effectively improving the photocatalytic degradation efficiency and stability.[12] The plasmonic effect refers to a range of optical, thermal, and electronic phenomena that arise from the coupling of photons with collective oscillations of free electrons in metals or materials with high free electron density. It has been widely utilized to significantly enhance photocatalytic performance by leveraging three key advantages: a large extinction cross-section, tunable resonant energy, and ultrasensitive sensing capabilities.[13,14] The Au@TiO_2 core–shell nanostructure catalyst developed by Chen *et al.*[15] demonstrates enhanced adsorption capacity and photocatalytic degradation efficiency through synergistic integration of the plasmonic effect from Au cores and interfacial charge transfer engineering in the heterostructure. The strategic integration of the plasmonic effect in Au/SnS_2 heterojunction photoelectrodes is expected to achieve remarkable enhancement in photodegradation efficiency.

In this paper, a gold-based tin sulfide self-supporting photoelectrode (SnS_2/Au) was fabricated on a titanium foil substrate

Shanxi College of Technology, Shuozhou, Shanxi Province, 036000, China. E-mail: tyy20220418@163.com

through a combination of ion sputtering and solvothermal methods. The surface morphology and optical behavior of the photoelectrode were comprehensively characterized using scanning electron microscopy (SEM), X-ray diffraction (XRD), X-ray photoelectron spectroscopy (XPS), ultraviolet-visible spectrophotometry (UV-vis), and fluorescence spectrophotometry (FL), respectively. The experimental results reveal that the SnS_2/Au heterostructure not only synergistically extends photon harvesting in the visible light region but also suppresses photoinduced electron–hole recombination, compared with monocomponent SnS_2 or Au catalysts. The photoelectrochemical degradation rate of RhB on the SnS_2–Au/Ti foil composite self-supporting photoelectrode reached 81.25% within 120 min, which was superior to that of the single SnS_2/Ti foil (72.80%) and the single Au/Ti foil electrode (43.07%). This work presents a novel approach to enhancing the photoelectric degradation of RhB through the utilization of the plasmon effect.

2 Experimental

2.1 Experimental reagents

Tin(IV) chloride pentahydrate ($SnCl_4 \cdot 5H_2O$), thioacetamide (C_2H_5NS), anhydrous sodium sulfite (Na_2SO_3), rhodamine B ($C_{28}H_{31}ClN_2O_3$), potassium chloride (KCl), and absolute ethanol (C_2H_6O) were all purchased from Shanghai Macklin Biochemical Technology Co., Ltd. The titanium foil and gold target (99.999%) were purchased from Zhongnuo New Materials (Beijing) Technology Co., Ltd. The deionized water used in the experiment was self-prepared by a pure water machine (TTL-6B). The reagents involved in the experiment were all directly purchased and used without further processing.

2.2 The preparation of SnS_2–Au/Ti foil self-supporting photoelectrode

The self-supported SnS_2–Au/Ti foil photoelectrode was successfully fabricated on the metal titanium substrate using the ion sputtering method and the solvothermal method, as illustrated in Scheme 1.

(1) The Au/Ti foil was prepared by the ion sputtering method. The titanium foil was cut into 2*4 cm rectangles, and it was cleaned with detergent powder, absolute ethanol, and deionized water for 30 minutes, respectively. Au thin films were deposited on Ti foils by magnetron sputtering (GVC-2000) under optimized conditions: a target–substrate distance of 2.5 cm, a current of 10 mA, and an Ar pressure of 4.00 Pa. By controlling the sputtering durations (40–200 s), Au_X/Ti electrodes (where X represents the deposition time in seconds) were fabricated. Unless otherwise specified, all Au/Ti foil electrodes mentioned in this study refer to those prepared with a sputtering time of 120 s.

(2) The SnS_2–Au/Ti foil photoelectrode was prepared by the solvothermal method. The as-prepared Au/Ti foil or pure Ti foil was immersed in a solution of absolute ethanol containing 50 mM C_2H_5NS and 25 mM $SnCl_4 \cdot 5H_2O$ in a 25 mL reaction vessel. The reaction vessel was then transferred to a vacuum drying oven at 80 °C, where it was allowed to react for 4 hours to prepare either the SnS_2–Au/Ti foil electrode or the SnS_2–Ti foil electrode.

2.3 Characterization

The crystal structure of the catalyst on the photoelectrode surface was analyzed by X-ray diffraction (XRD, MiniFlex600). The scanning range was set from 20° to 80°, and the scanning speed was set at 10° min^{-1}. Microscopic morphology and structure were analyzed by using a scanning electron microscope (SEM, JSM-7800F). The elemental composition and valence state were analyzed by X-ray photoelectron spectroscopy (XPS, Thermo ESCALAB 250). The optical behavior of the self-supporting photoelectrode was analyzed using an ultraviolet-visible spectrophotometer (UV-vis, UV-690) and a fluorescence spectrophotometer (FL, F-7000). The excitation light wavelength of FL spectrophotometer was set to 410 nm.

2.4 Photoelectrochemical degradation of RhB measurements

The standard three-electrode system was employed as the photoelectrochemical degradation cell. The CHI 760E instrument served as the electrochemical workstation, and the degradation bias was set at 0.3 V *vs.* SCE. Specifically, the as-prepared photoelectrode, the saturated calomel electrode, and the platinum sheet were used as the working electrode, the reference electrode, and the counter electrode, respectively. A mixed solution of 20 mM Na_2SO_3, 0.5 M KCl, and 4 mg L^{-1} RhB was used as the degradation solution. Visible light irradiation was provided by xenon lamps (CEL-HXF300), and the

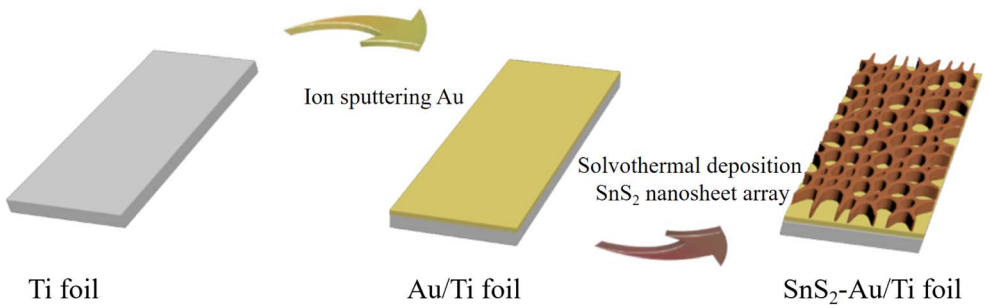

Scheme 1 Schematic illustration of the synthesis process of SnS_2–Au/Ti foil self-supporting photoelectrode.

concentration of RhB during the degradation process was monitored using the ultraviolet-visible spectrophotometer (752G, Shanghai Yidian).

3 Results and discussion

3.1 Structure characterization

Fig. 1a–f presents the SEM images of the Ti foil, Au/Ti foil, SnS_2/Ti foil, and SnS_2–Au/Ti foil electrodes, respectively. The SEM image of Ti foil depicts a surface with relatively low roughness (shown in Fig. 1a). Fig. 1b corresponds to the Au/Ti foil electrode, demonstrating that gold nanoparticles are uniformly distributed on the titanium metal substrate. Fig. 1c and d is associated with the SnS_2/Ti foil electrode, where the as-prepared SnS_2 nanosheet arrays are evenly deposited on the titanium metal substrate, exhibiting a pore size of approximately 200 nanometers. The SEM images of the SnS_2–Au/Ti foil (shown in Fig. 1e and f) are similar to those of the SnS_2/Ti foil, suggesting that the incorporation of an intermediate Au nanoparticle layer does not affect the morphology of SnS_2.

Elemental mapping images of SnS_2–Au/Ti foil are illustrated in Fig. $1g_{1-3}$, showing uniform distributions of S, Au, and Sn elements on the titanium substrate. Furthermore, the energy-dispersive X-ray spectroscopy (EDX) analysis was employed to analyze the atomic content of corresponding elements (Fig. 1h). The results indicate that the SnS_2–Au/Ti foil electrode is predominantly composed of Sn, S, and Au elements, with an atomic ratio of Sn to S approximately equal to 1 : 2, confirming the formation of SnS_2. Notably, Au accounts for only 1.63% of the total elemental composition of the SnS_2–Au/Ti foil electrode. Besides, the EDX spectra of Ti foil, Au_{120}/Ti foil and Au_{200}/Ti foil were displayed in Fig. S1. It is evident that the gold content on the electrode surface increases with prolonged ion sputtering duration.

The crystal structure of the prepared electrode has been characterized, as depicted in Fig. 2. The diffraction peaks at 44.37° and 64.56° are indexed to (200) and (220) planes of Au, respectively (JCPDS card no. 89-3697). Obviously, the XRD diffraction peaks of Au nanoparticles for the Au_X/Ti foil electrode become sharper with an extended sputtering duration, as shown in Fig. 2a. Besides, the diffraction peaks at 15.05°, 30.38°, 50.11°, and 58.55° correspond to the (001), (002), (110), and (200) planes of SnS_2, respectively (JCPDS card no. 83-1705).

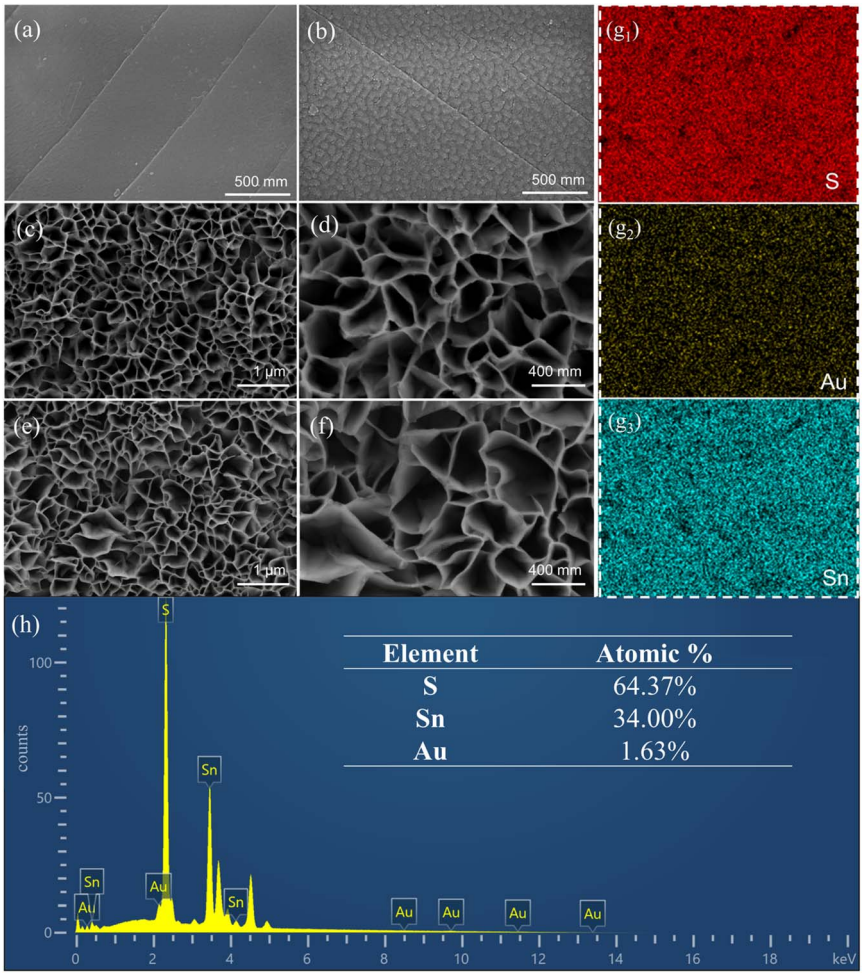

Fig. 1 SEM images of (a) Ti foil electrode, (b) Au/Ti foil electrode, (c and d) SnS_2/Ti foil electrode and (e and f) SnS_2–Au/Ti foil electrode, respectively. (g_{1-3}) Elemental mapping images and (h) EDX spectra of SnS_2–Au/Ti foil electrode.

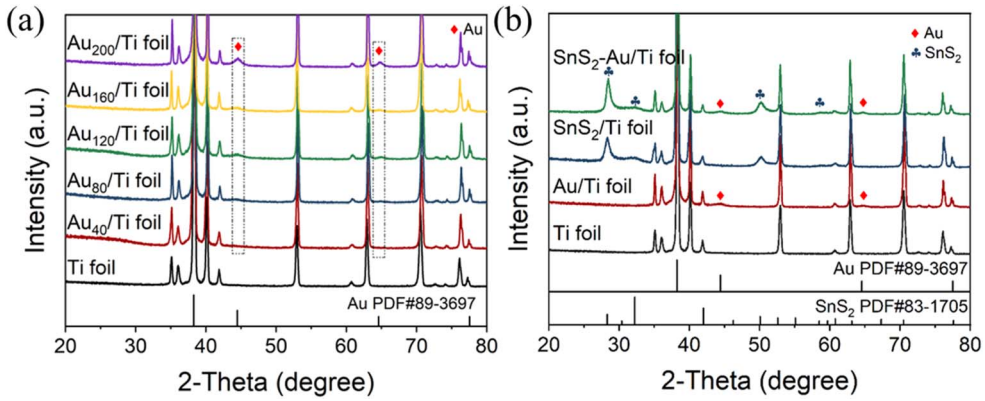

Fig. 2 XRD patterns of (a) the Au_X/Ti foil electrodes prepared with different sputtering durations, (b) SnS_2–Au/Ti foil, Au/Ti foil, SnS_2/Ti foil and Ti foil electrodes.

Additionally, the remaining diffraction peaks can be attributed to the titanium metal substrate. A comparison of the XRD diffraction patterns for the SnS_2–Au/Ti foil, Au/Ti foil, SnS_2/Ti foil, and Ti foil electrodes (Fig. 2b) clearly demonstrates that SnS_2 can be effectively synthesized on both Au/Ti foil and Ti foil substrates *via* the solvothermal method.

The XPS analysis was performed on the SnS_2–Au/Ti foil electrode to characterize the elemental composition and valence state, as shown in Fig. 3. It is obvious that the SnS_2–Au/Ti foil electrode contains the primary elements of Sn, S, and Au (as shown in Fig. 3a). In Fig. 3b, the peaks at 161.7 and 162.9 eV are attributed to S^{2-} $2p_{3/2}$ and S^{2-} $2p_{1/2}$, respectively. The peaks at 486.8 and 495.2 eV correspond to Sn^{4+} $3d_{5/2}$ and Sn^{4+} $3d_{3/2}$, respectively (Fig. 3c).[16–18] Furthermore, the weak peaks of Au $4f_{7/2}$ and Au $4f_{5/2}$ are located at 84.2 and 87.6 eV, respectively (Fig. 3d).[19,20]

3.2 Optical property

The optical behavior of self-supported photoelectrodes serves as a critical factor influencing the photoelectrocatalytic degradation performance. The UV-vis absorption spectra and FL emission spectra of SnS_2–Au/Ti foil, Au/Ti foil, and SnS_2/Ti foil electrodes were illustrated in Fig. 4. Obviously, the as-prepared Au/Ti foil displays a noteworthy absorption peak near 560 nm, which is indicative of the localized surface plasmon resonance (LSPR) effect (Fig. 4a).[21,22] For the SnS_2/Ti foil electrode, the absorption peak observed at 580 nm can be attributed to the intrinsic bandgap (2.2 eV) of the SnS_2 semiconductor.[23] Furthermore, the light absorption of the as-prepared SnS_2–Au/Ti composite self-supported photoelectrode exhibits a red shift, indicating that the plasmonic effect of the Au layer can effectively synergize with the inherent light absorption properties of the SnS_2 semiconductor, leading to an enhancement in the overall light absorption capacity of the self-supported SnS_2–Au/Ti composite photoelectrode within the visible light spectrum.

As shown in Fig. 4b, the FL emission spectra of the as-synthesized electrodes are illustrated, with the peak intensity at 600 nm being proportional to the recombination probability of photogenerated carriers.[24] The Au/Ti foil electrode exhibits a substantially higher FL emission peak in comparison to the SnS_2–Au/Ti foil and SnS_2/Ti foil electrodes. This phenomenon can be attributed to the plasmonic effect of Au, which generates photogenerated carriers in significantly higher magnitudes and causes much faster recombination than those in semiconductor materials.[25] Most importantly, the SnS_2–Au/Ti foil electrode exhibits much lower emission intensity, revealing that the synergistic effect of SnS_2 and Au significantly reduces the recombination of photogenerated carriers.

3.3 Photoelectrochemical degradation of RhB measurements

Fig. 5a presents the photoelectrocatalytic degradation performance test results of SnS_2–Au/Ti composite electrodes, which were fabricated by *in situ* growing SnS_2 nanosheet arrays on Au_{40}/Ti foil, Au_{80}/Ti foil, Au_{120}/Ti foil, Au_{160}/Ti foil, and Au_{200}/Ti foils, respectively. It can be observed that the photoelectrocatalytic degradation performance of the composite electrode initially increases with the prolongation of the sputtering time of Au nanoparticles and subsequently decreases. The SnS_2–Au_{120}/Ti foil composite electrode exhibits the highest photoelectric degradation efficiency for RhB within 120 min, achieving a degradation rate of 81.25%. The photo response current density serves as a key indicator for evaluating the photoelectrocatalytic performance of the photoelectrode. As illustrated in Fig. 5b, the *J*–*t* curves depict the behavior under a constant bias of 0.3 V *vs.* SCE in the same photoelectrochemical degradation cell, measured under intermittent illuminated and dark conditions. The Au/Ti foil electrode shows a weak photoelectric response due to the plasmonic effect of Au nanoparticles, but exhibits the lowest photoelectric response among the samples because of limited active reaction sites. When the tin disulfide semiconductor was synergistically integrated with the Au nanoparticles, the photo response current density reaches its maximum, indicating optimal photoelectrocatalytic performance of the SnS_2–Au/Ti foil electrode.

Fig. 5c illustrates the photoelectrocatalytic, photocatalytic, and electrocatalytic degradation performance of the SnS_2–Au/Ti

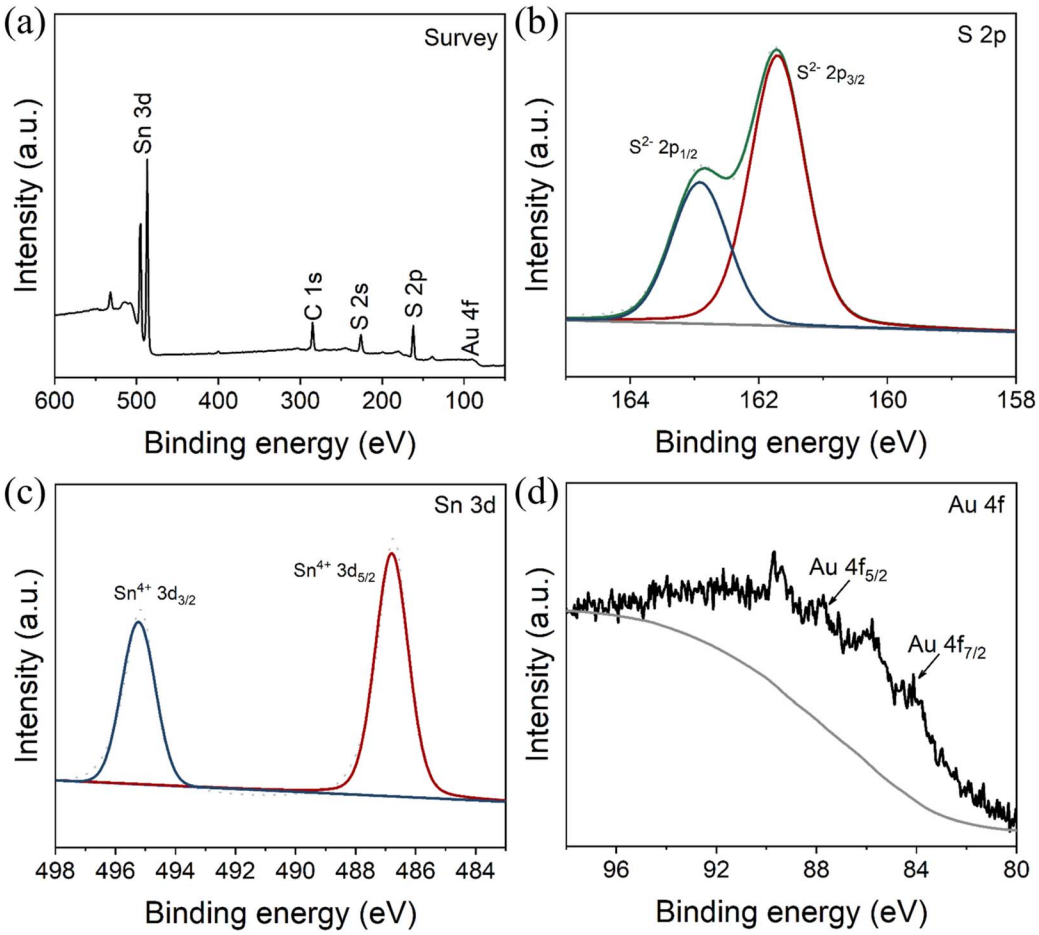

Fig. 3 XPS spectrum of the SnS_2–Au/Ti foil, (a) survey spectra and high-resolution XPS (HRXPS) spectrum of (b) S 2p, (c) Sn 3d, and (d) Au 4f.

foil composite electrode under identical testing conditions. Within 120 min, the pure electrocatalytic degradation and photocatalytic degradation efficiencies of the SnS_2–Au_{120}/Ti foil composite electrode are 45.59% and 68.99%, respectively, both of which are lower than its photoelectrocatalytic degradation efficiency. Furthermore, the repeated photoelectrocatalytic degradation performance was also tested to evaluate the stability of the composite electrode, as displayed in Fig. 5d. It can be clearly observed that the degradation rate of the electrode reached approximately 85% within 120 minutes in five repeated experiments, and then stabilized in the third test cycle. This stabilization might be due to the excessive catalyst

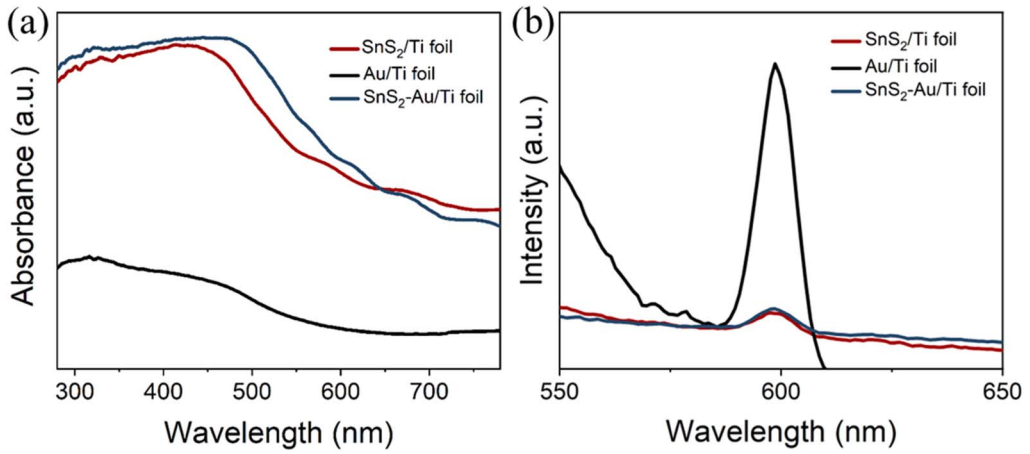

Fig. 4 (a) UV-vis absorption spectra and (b) FL emission spectra of SnS_2–Au/Ti foil, Au/Ti foil, and SnS_2/Ti foil electrodes.

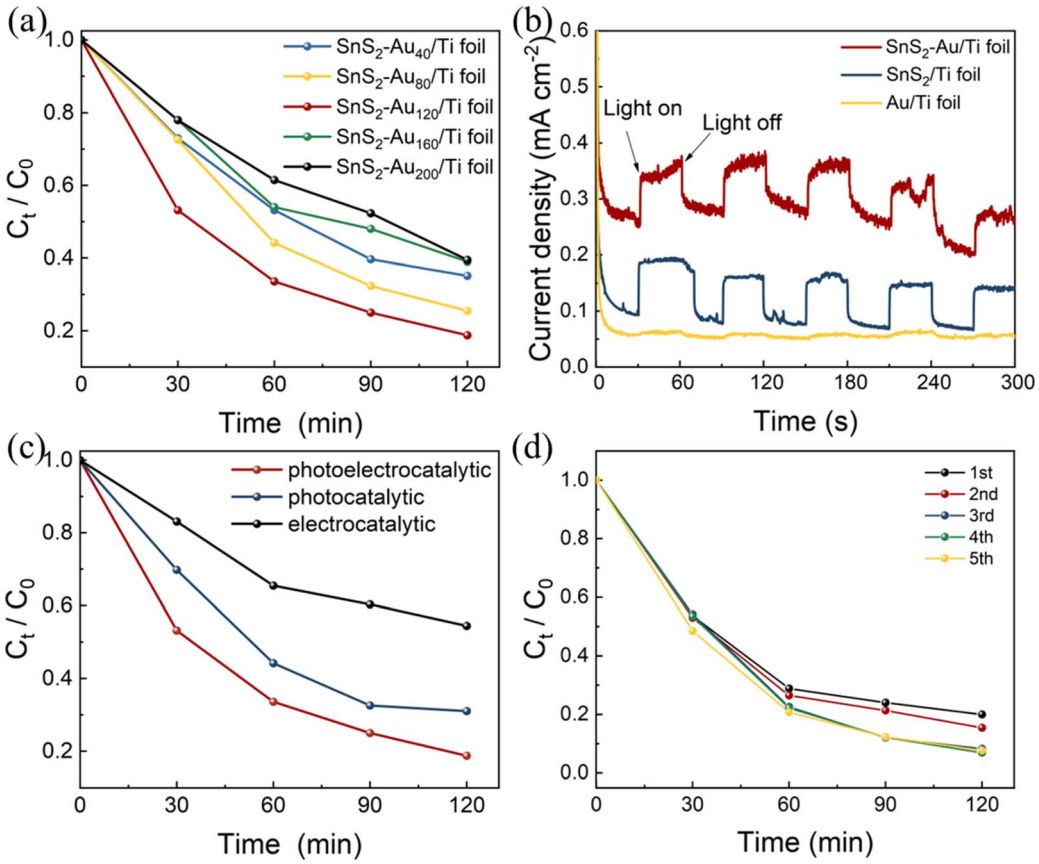

Fig. 5 (a) Photoelectrocatalytic degradation performance of RhB on SnS_2–Au_X/Ti foil electrodes prepared by varying durations of Au ion-sputtering. (b) *J*–*t* curves of SnS_2–Au/Ti foil, Au/Ti foil, and Ti foil electrodes under a bias of 0.3 V *vs.* SCE under intermittent dark and illumination conditions. (c) Comparison of the RhB degradation performance *via* photoelectrocatalytic, photocatalytic, and electrocatalytic degradation and (d) the repeated photoelectrocatalytic degradation performance of RhB on SnS_2–Au/Ti foil electrode.

shedding from the surface of the composite electrode during the first two degradation cycles.

To further investigate the origin of the photoelectrocatalytic degradation performance of RhB using the SnS_2–Au/Ti foil composite electrode, the Ti foil, SnS_2/Ti foil, and Au/Ti foil electrodes were individually evaluated under the same testing conditions, as illustrated in Fig. 6a. The degradation rate of the bare Ti foil substrate was about 7.74% within 120 min, which might be attributed to the adsorption effect of the metal substrate on RhB.[26] Besides, the SnS_2–Au/Ti foil composite

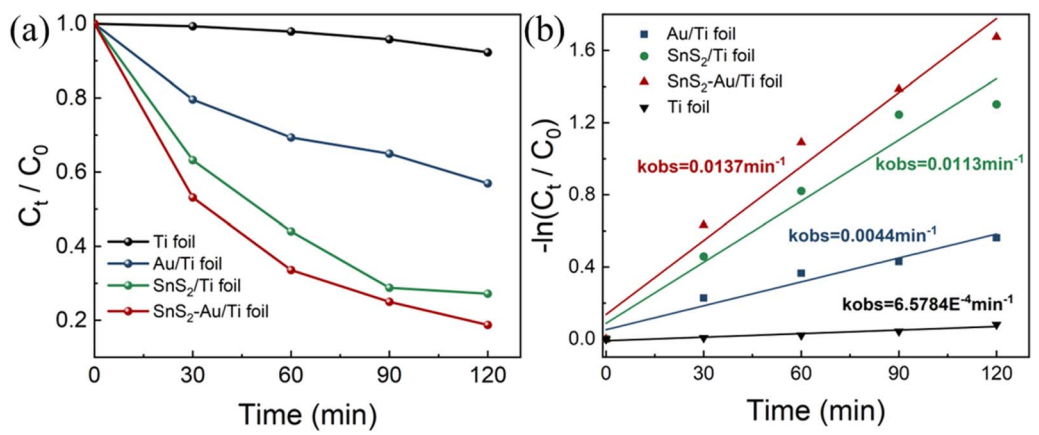

Fig. 6 (a) Photoelectrocatalytic degradation performance and (b) corresponding kinetic curves of Ti foil, SnS_2/Ti foil, Au/Ti foil, and SnS_2–Au/Ti foil electrodes, respectively.

electrode exhibits a degradation rate of 81.25%, demonstrating an enhancement of 88.87% and 11.59% compared to the pure Au/Ti foil electrode (43.02%) and the SnS_2/Ti foil electrode (72.81%), respectively. Besides, the pseudo-first-order kinetic model was employed to analyze the degradation kinetics of RhB on various photoelectrodes, as illustrated in Fig. 6b. Among them, the degradation rate of SnS_2–Au/Ti foil composite electrode was the highest, reaching 0.0137 min^{-1}, which was higher than that of Ti foil (0.0006 min^{-1}), SnS_2/Ti foil (0.0113 min^{-1}), and Au/Ti foil (0.0044 min^{-1}) electrodes. It is evident that the SnS_2–Au/Ti foil composite electrode has the strongest photoelectrocatalytic degradation activity. Thus, the experimental results demonstrate that the SnS_2–Au/Ti foil composite electrode, fabricated by loading SnS_2 nanosheet arrays onto a bottom layer of Au nanoparticles, can achieve both the plasmonic effect of Au and the semiconductor photocatalytic effect of SnS_2. This effectively enhances the photoelectric degradation process, thereby promoting the degradation of RhB.

4. Conclusions

In summary, we successfully fabricated the SnS_2–Au/Ti foil composite self-supporting photoelectrode on a titanium metal substrate through the combination of ion sputtering and solvothermal methods, and demonstrated its application in the photoelectrocatalytic degradation of RhB. The experimental results demonstrate that the synergistic integration of the plasmonic effect in Au with the semiconductor inherent characteristics of SnS_2 enables the composite electrode to exhibit enhanced performance in photoelectrocatalytic degradation of RhB. Under a constant potential of 0.3 V, the system achieves a degradation efficiency of 81.25% within 120 minutes. This strategy of enhancing the semiconductor photodegradation performance *via* the synergy of the plasmonic effect offers a novel perspective for the investigation of pollutant photodegradation.

Conflicts of interest

There are no conflicts to declare.

Data availability

All relevant data are within the manuscript and its additional files.

Supplementary information: the EDS spectrum (EDS) of SnS_2–Au/Ti foil electrode. See DOI: **https://doi.org/10.1039/d5ra04205d**.

Acknowledgements

This study has been financially supported by Fundamental Research Program of Shanxi Province (Grant No. 202203021222328) and Research Initiation Fund Programs of Shanxi College of Technology (Grant No. 200101).

References

1 D. Xu and H. L. Ma, Degradation of rhodamine B in water by ultrasound-assisted TiO_2 photocatalysis, *J. Cleaner Prod.*, 2021, **313**, 127758–127764.
2 X. C. Du, J. H. Zhu, Z. J. Quan, *et al.*, Adsorption of rhodamine B by organic porous materials rich in nitrogen, oxygen, and sulfur heteroatoms, *New J. Chem.*, 2021, **45**, 3448–3453.
3 P. S. Priya, P. P. Nandhini, S. Vaishnavi, *et al.*, Rhodamine B, an organic environmental pollutant induces reproductive toxicity in parental and teratogenicity in F1 generation in vivo, *Comp. Biochem. Physiol., Part C: Toxicol. Pharmacol.*, 2024, **280**, 109898–109910.
4 Q. W. Zheng, X. Liu, L. T. Tian, *et al.*, Mechanism of Fenton catalytic degradation of Rhodamine B induced by microwave and Fe_3O_4, *Chin. Chem. Lett.*, 2025, **36**, 109771–109780.
5 L. X. Wang, X. L. Liu, R. Zhang, *et al.*, Synthesis of Zeolite-Based Cu/Fe-X from Coal Gangue for Fenton-Like Catalytic Degradation of Rhodamine B, *J. Inorg. Organomet. Polym. Mater.*, 2024, **34**, 722–734.
6 D. P. Wu, F. F. Li, Q. Chen, *et al.*, Mediation of rhodamine B photodegradation by biochar, *Chemosphere*, 2020, **256**, 127082–127088.
7 O. N. Nkwachukwu, C. Muzenda, K. D. Jayeola, *et al.*, Photoelectrocatalytic Degradation of Methylene Blue on Electrodeposited Bismuth Ferrite Perovskite Films, *Materials*, 2023, **16**, 2769–2790.
8 Z. H. Guo, G. Q. Wang, H. Q. Fu, *et al.*, Photocatalytic degradation of methylene blue by a cocatalytic PDA/TiO_2 electrode produced by photoelectric polymerization, *RSC Adv.*, 2020, **10**, 26133–26141.
9 C. B. Tang, P. Huang, Z. L. Liu, *et al.*, Improved photoelectrocatalytic degradation of methylene blue by $Ti_3C_2T_x$/$Bi_{12}TiO_{20}$ composite anodes, *Ceram. Int.*, 2022, **48**, 24943–24952.
10 G. Matyszczak, P. Jozwik, E. Polesiak, *et al.*, Sonochemical preparation of SnS and SnS_2 nano- and micropowders and their characterization, *Ultrason. Sonochem.*, 2021, **75**, 105594–105603.
11 X. F. Shuai, Y. Wang, J. Zhang, *et al.*, Mn-Dependent Morphology and Structure of SnS_2 Nanosheets and the Photocatalytic Performance, *ChemistrySelect*, 2022, **7**, 202201068–202201076.
12 J. Chen, B. X. Wang, J. C. Wang, *et al.*, Development of a new high-performance visible-light photocatalyst by modifying tin disulfide with cyclized polyacrylonitrile, *Mater. Lett.*, 2023, **330**, 133353–133357.
13 K. A. Dahan, Y. Li, J. Xu, *et al.*, Recent progress of gold nanostructures and their applications, *Phys. Chem. Chem. Phys.*, 2023, **25**, 18545–18576.
14 M. L. Xue, W. Mao, J. S. Chen, *et al.*, Application of Au or Ag nanomaterials for colorimetric detection of glucose, *Analyst*, 2021, **146**, 5726–5740.
15 J. Q. Chen, Y. J. Chen, J. T. Shuai, *et al.*, Enhancement of visible light adsorption and photocatalytic degradation

activity of organic dye by coating semiconducting TiO_2 shell on plasmonic Au particles, *J. Alloys Compd.*, 2024, **1009**, 176938–176945.

16 J. Sakthivel and A. R. Warrier, Ultrasound assisted reductive degradation of toxic textile dye effluents using Sn nanoparticles, *Mater. Chem. Phys.*, 2022, **278**, 125610–125619.

17 D. Kim, J. Park, J. Choi, *et al.*, Compositional ratio effect on the physicochemical properties of SnSe thin films, *Phys. B*, 2021, **612**, 412890–412896.

18 P. Parameswari and A. Sakthivelu, Microwave-Assisted Green Process of Cobalt Ferrous Codoped Tin Oxide Nanoparticles: Antibacterial, Anticancer, and Toxicity Performance, *BioNanoScience*, 2022, **12**, 1211–1219.

19 Z. Wang, X. H. Wang, M. Z. Yun, *et al.*, Polyethyleneimine modified Au core Rh shell nanodendrites for light-promoted nitrite reduction reaction at low concentration, *J. Energy Chem.*, 2025, **103**, 400–407.

20 A. Mellor, A. Wilson, C. L. Pang, *et al.*, Photoemission core level binding energies from multiple sized nanoparticles on the same support: TiO_2(110)/Au, *J. Chem. Phys.*, 2020, **152**, 024709–024715.

21 Y. Y. Gao, Q. H. Zhu, J. F. Zhao, *et al.*, Regulating Charge Separation Via Periodic Array Nanostructures for Plasmon-Enhanced Water Oxidation, *Adv. Mater.*, 2025, **37**, 2414959–2414964.

22 Y. Y. Zhou, J. Y. Wu, W. B. Cui, *et al.*, Molecular sieve redefines SPR sensible range for "win-win" dual functions to enhance the sensitization and anti-fouling, *Nano Today*, 2025, **61**, 102670–102680.

23 X. W. Guo, F. Zhang, Y. C. Zhang, *et al.*, Review on the Advancement of SnS_2 in the Photocatalysis, *J. Mater. Chem. A*, 2023, **11**, 7331–7343.

24 Y. Y. Tian, Y. Song, J. J. Liu, *et al.*, MoSx Coated Copper Nanowire on Copper Foam as A Highly Stable Photoelectrode for Enhanced Photoelectrocatalytic Hydrogen Evolution Reaction via. Plasmon-Induced Hot Carriers, *Chem. Eng. J.*, 2020, **398**, 125554–125564.

25 R. S. Haider, S. Y. Wang, J. F. Zhao, *et al.*, Prominence of copper in AuCu alloy towards enhance surface plasmon resonance-driven water oxidation, *Nano Energy*, 2025, **133**, 110499–110510.

26 Y. H. Chen, D. Zhao, T. Q. Sun, *et al.*, The preparation of MoS_2/δ-FeOOH and degradation of RhB under visible light, *J. Environ. Chem. Eng.*, 2023, **11**, 110353–110364.